RSC Advances

ROYAL SOCIETY OF CHEMISTRY

www.rsc.org/advances

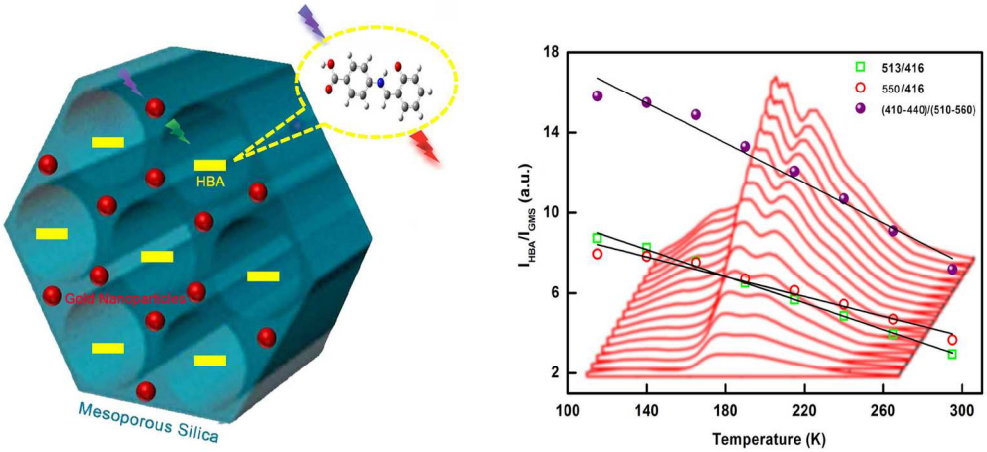

225x99mm (268 x 277 DPI)

Journal Name

ARTICLE

Salicylideneanilines Encapsulated Mesoporous Silica Functionalized Gold Nanoparticles: A Low Temperature Calibrated Fluorescent Thermometer

Received 00th January 20xx,
Accepted 00th January 20xx

DOI: 10.1039/x0xx00000x

www.rsc.org/

Jian Wu,[a b] Qingmei Cheng,[c] Wei zhou,[d] Zhihong Wei,[b] and Jinglei Yang*[a]

In this study, a novel temperature responsive fluorescence sensor, 4-(2-hydroxybenzylideneamino) benzoic acid (HBA), encapsulated in the nanochannel of mesoporous silica functionalized gold nanoparticles (GMS) was synthesized and studied. The fluorescence intensity of HBA-GMS showed excellent linear temperature sensitivity over a wide range from cryogenic to room temperature (100-298 K). Meanwhile, GMS was used as immobilization matrix to improve the light harvesting and calibrate HBA fluorescence intensity at different temperature because of the stable and insensitive fluorescent signal of gold nanoparticle intercalated into the walls of GMS. In addition, it was found HBA-GMS exhibits excellent biocompatibility and low toxicity for cellular imaging due to robust GMS supports. The results suggest that the assembled mesostructure provides a promising intelligent calibrated fluorescent thermometer with potential applications in sensor and cryogenic bio-detection and therapy fields.

Introduction

Temperature is the very important measured physical property in industrial and scientific fields. Among the numerous methods to determine temperature, fluorescence measurement as sensor has attracted much attention in the past few years, for they are accurate, easy-observable detection and more sensitive signals.[1, 2] Recently, some temperature-sensitive fluorescence materials as sensors, such as nanotube-based systems, quantum dots, and organic dyes, have been used to measure temperature over a wide range.[3-9] Particularly, organic molecules are attractive candidates to sense temperature, especially because their broad excitation profiles, large absorption cross sections, and tunable emission energies.[10-14] However, the development of efficient and signal stable fluorescence-base temperature sensor over a wide range temperature, especially in ultra-low temperature, remains a critical scientific challenge.

Recently, salicylideneaniline and its derivatives have been reported, which exhibits thermochromism and photochromism in the solid state. This phenomenon can be explained by taking account of the photo and thermal induced change of fluorescence.[15-20] Most salicylideneaniline exist mainly as the cis-keto form at room temperature in the solid state. However, the population of the cis-keto form decreases and that of the enol form increases with temperature decreasing. Furthermore, the excited S_1 state will generate a hot cis-keto* vibrational state. The hot cis-keto* form in the S_1 state may easily convert to the cis-keto* form in S_1 state because the hot cis-keto* form have higher vibrational energy. Hence, the cis-keto* and hot cis-keto* forms are two vibrational states influenced by temperature, following the Boltzmann distribution law.[21, 22] Thus, we firstly choose salicylideneaniline with two reverse cis-keto tautomer as thermal responsive fluorescent candidates for thermometers in a wide temperature range.

On the other hand, although numerous organic molecules have been reported with intense fluorescence, the common organic molecules have two important drawbacks including rather poor optical signal stability and high toxicity.[23, 24] Common fluorescence system could not be used in both solid and solution system due to the solubility of the probes, which are affected by its microenvironments and easily impaired or even lost.[25, 26] Besides, potential toxicity about organic dye, which would cause undesirable dangerous interactions with biological cells with potential for generating toxicity, has been reported. Thus, the chemical stability and toxicity of organic materials have to be investigated to ensure they are safe for medical applications. More importantly, the optical signals from the temperature sensors ideally should be stable and undisturbed under the complex biological conditions.[27] To overcome these drawbacks and to avoid the disturbance from the surroundings, an appropriate approach involving encapsulation has been proved to be effective.[27-29] Therefore,

[a] School of Mechanical and Aerospace Engineering, Nanyang Technological University, Nanyang 639798, Singapore.
[b] State Key Laboratory of Coal Conversion, Institute of Coal Chemistry, Chinese Academy of Sciences, Taiyuan, Shanxi 030001, P. R. China.
[c] Department of Chemistry, Merkert Chemistry Center, Boston College, Chestnut Hill, MA 02467. USA.
[d] Hefei National Laboratory for Physical Sciences at the Microscale University of Science and Technology of China, Hefei
Corresponding author's email: E-mail: mjlyang@ntu.edu.sg

† Electronic Supplementary Information (ESI) available: Experimental section and Additional experimental data. See DOI: 10.1039/x0xx00000x

it is vital to pursue ideal and suitable supports to encapsulate organic molecules to improve their optical stability and biocompatibility as well as ratiometric fluorescence signal. Furthermore, dual emission fluorescence systems have also been developed to improve ratiometric fluorescence signal to avoid the disturbance of optical signals from the surroundings. Recently, some papers have reported the dual emission by polymer dots, semiconductor nanocrystals and molecular beacons as calibrated parts, which are temperature insensitive.[34] In this study, we have firstly designed ratiometric temperature sensors with two emission peaks by gold nanoparticle as calibrated fluorescence part.

Recently, mesoporous silica as scaffolds have been receiving greater attention due to their well-ordered mesoporous structure, large pore diameter and high surface area, which facilitate the possibility of encapsulating and delivering large quantities of small molecules.[30, 31] Especially, Ryan group has recently reported a mesoporous silica hybrid material (GMS) with gold nanoparticles in the silica walls of GMS.[32, 33] The highly pore order and morphology can be controlled very well and the gold nanoparticles are highly dispersed into the silica walls of GMS. The abundant hydroxyl groups on the pore surface make these materials interact well with the organic molecules. Thus, encapsulation of organic molecule enhances their stability and performance in physiological conditions. In addition, since gold nanoparticles with emission features are temperature insensitive, it allows the design of temperature calibrated fluorescent sensor by single wavelength excitation.[34]

Inspired by aforementioned concepts, to address the need for robust and calibrated fluorescent temperature sensing, we describe a novel temperature sensitive dye molecules, 4-(2-hydroxybenzylideneamino)benzoic acid (HBA), which is encapsulated within mesoporous silica functionalized gold nanoparticles hybrid material (GMS). HBA-GMS show excellent linear temperature sensitivity from 100 to 298 K. GMS not only improves the chemical stability, but also attenuates the intrinsic toxic effect of HBA. Moreover, the HBA-GMS could be as ratiometric and calibrated temperature sensor, because the HBA fluorescence intensity can be calibrated by GMS in a wide temperature range, which the GMS fluorescence signals is temperature insensitive. Thus, the superstructures design would offer a new approach to construct highly sensitive and selective sensors and cryogenic thermometer.

Results and discussion

In this work, we report a novel gold nanoparticles and mesoporous silica hybrid material (GMS) with assembled 4-(2-hydroxybenzylideneamino) benzoic acid (HBA), called HBA-GMS, which is synthesized by a simple two steps method.[37] The first step involves the both syntheses of HBA and GMS according to previously reported methods (see the Supporting Information S1). Firstly, under vacuum condition, impurities and air trapped inside the GMS are completely removed. Then, the GMS by vacuum treated and protonated are immersed in the aqueous solution with HBA for 12 hours. Meanwhile, the

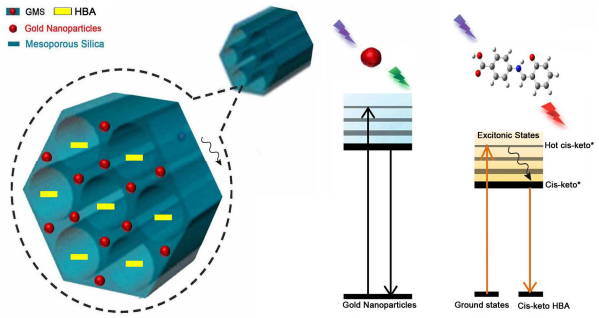

Scheme 1. Schematic representation of HBA assembled within the mesoporous of GMS. And the different electronic structures related to fluorescence of HBA (cis-keto) and gold nanoparticles leading to dual emission.

HBA molecules are infiltrated into the nanochannels of GMS by capillary forces. This nanostructure is denoted by HBA-GMS. In this process, -SiOH groups are protonated to positively charge -OH. Meanwhile, HBA molecules are negatively charged to -SiOH. HBA molecules are absorbed onto the surface of GMS. Thus, HBA assembles on the positively charged surface of the nanochannels to form anchored HBA molecules as indicated in Scheme 1.

The powder X-ray diffraction (XRD) patterns of GMS are shown in FigureS2a. GMS are highly ordered, showing two strong diffraction peaks for the 111 and 200 planes. From the XRD patterns, the average crystallite sizes of gold nanoparticle are calculated by the Scherrer equation using the most intense (111) XRD peak. The calculated crystallite size of gold nanoparticle is about 2.3 nm in agreement with the size reported previously (see the Supporting Information S2).[39] FigureS3 shows a UV-vis absorption spectrum of GMS with a peak at 530 nm, which indicate an average particle diameter of less than 5.0 nm. The nitrogen adsorption-desorption isotherms of GMS are shown in FigureS2b. The pore diameter, specific surface area and Barrett-Joyner-Halenda (BJH) pore volume of GMS are 4.7 nm, 539 m^2 g^{-1} and 0.52 cm^3 g^{-1}, respectively. The isotherms of GMS are of type IV, which is typical for mesoporous structure.[40] Above results indicates that GMS possesses typical mesoporous structure similar to SBA-15 and is suitable to encapsulate small molecules to improve their chemical stability.

Furthermore, Figures 1a and 1b show transmission electron microscopy (TEM) images of HBA-GMS and GMS, respectively. As can be seen, the GMS displayed highly ordered nanochannels with a channel diameter of ~4.7 nm and a wall thickness of ~2.2 nm (Figure1b), consistent with the two

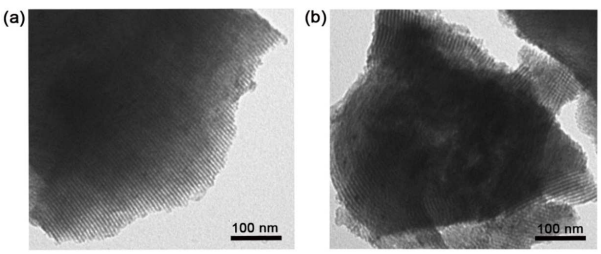

Figure1. TEM images of HBA-GMS (a) and GMS (b).

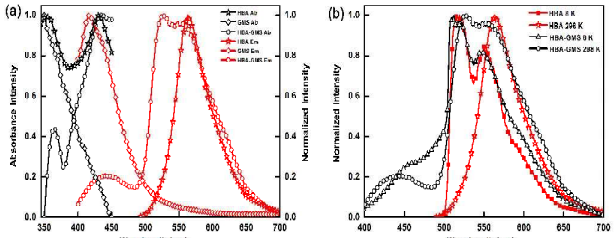

Figure2. (a) Measured absorption of HBA (hollow star), GMS (hollow circle) and HBA-GMS (hollow triangle) and fluorescence emission spectra of HBA (hollow star), GMS (hollow square) and HBA-GMS (hollow circle) at 298 K. (b) Fluorescence emission spectra of HBA (8 K, solid square; 298 K, hollow star) and HBA-GMS (8 K, hollow triangle; 298 K, hollow circle) at 8 and 298 K. The excitation wavelength is 390 nm.

dimension hexagonal mesostructure of SBA-15, in agree with nitrogen adsorption-desorption isotherms data (FigureS2b). The gold nanoparticles are well protected and segregated by silica walls of GMS even after calcination at high temperatures. Furthermore, the transmission electron microscopy (TEM) image provides a direct observation of the morphology and distribution of HBA-GMS and GMS, indicating that the nanochannels of HBA-GMS remains uniform as well as morphology of GMS. The diameter and shape of the channels of HBA-GMS are as regular as that of the GMS. The wall thickness of the HBA-GMS is ~2 nm, which is similar with the wall thickness of GMS. The results show that HBA molecules highly disperse into the channels of GMS, and HBA does not damage the textural and structure properties of GMS supports (Figure1b).

To further confirm the presence of HBA within the GMS and its amount, corresponding Fourier transform infrared (FTIR) spectra and thermogravimetric analysis (TGA) of HBA, GMS and HBA-GMS samples are compared as shown in FigureS4. It can be seen that a series of characteristic bands of the HBA at C-O band (1287 cm^{-1}) and aromatic C=C band (1569 and 1600 cm^{-1}) are present in the spectra of both HBA and HBA-GMS in agreement with previously reported for the HBA (FigureS4a).[38] The results also demonstrate that HBA has been successfully assembled into the nanochannels of GMS. Moreover, the weight percentage of HBA in HBA-GMS is estimated by thermogravimetric analysis (TGA) as shown in FigureS4b. The amount of HBA in hybrid HBA-GMS is estimated to be ~28 wt% by TGA.

To further assess the optical properties, the samples are characterized by spectra measurement. Figure2a shows the absorption and emission spectra of HBA, GMS and HBA-GMS at 298K. HBA and HBA-GMS show two adsorption peaks at 365 nm and 430 nm at 298 K, respectively. Moreover, the samples are also characterized by fluorescence spectra measurement. HBA and GMS exhibit emission peaks at 564 nm and 416 nm at 298 K when excited at 390 nm, respectively. HBA-GMS exhibits two emission peaks at an around 410-440 nm and an wide band at 510-560 nm at 298 K when excited at 390 nm. The peak at 410-440 nm is therefore contributed to the emission spectra of GMS. The latter broad peak at 510-560 nm is contributed to the emission spectra of HBA. Furthermore, we measure the emission spectra of HBA and HBA-GMS at 8 and 298 K as shown in Figure2b, respectively. In case of HBA, a narrow emission peak at 564 nm is observed at 298 K and a new peak at around 520 nm is observed with lower temperature of 8 K in similar with the results reported previously.[38] As we can be seen for HBA-GMS, the wide peak at 510-560 nm will splits into two emission peaks with decreasing temperature. Moreover, the two emission peaks are observed more obviously at temperatures ranging from 298 K to 8 K as shown in Figure 3a. At low temperature of 8 K, this wide peak at 510-560 nm splits into two obvious peaks at about 513 nm and 550 nm, which are similar with the optical behavior of HBA (Figure 2b).[38]

To evaluate the temperature-induced fluorescence intensity change of the HBA-GMS, fluorescence spectra of HBA-GMS are measured at different temperatures. Figure3a shows the fluorescence spectra of HBA-GMS at temperatures ranging from 8 to 298 K when excited at 390 nm. As can be seen, a gradual decrease in the fluorescence intensity with increasing temperature can be observed. The emission peak shifts towards longer wavelength from 510 to 560 nm with increased temperature. HBA-GMS show strong temperature-dependent fluorescence with a very high quantum yield from 8 to 298 K over a wide temperature range as shown in Table S1. The total quantum yields of the fluorescence are 0.76 and 0.2 at 8 and 298 K, respectively.

Furthermore, we have plotted the change in the fluorescence intensity of wavelength of 416, 513 and 550 nm peaks and the integrated PL intensity as a function of

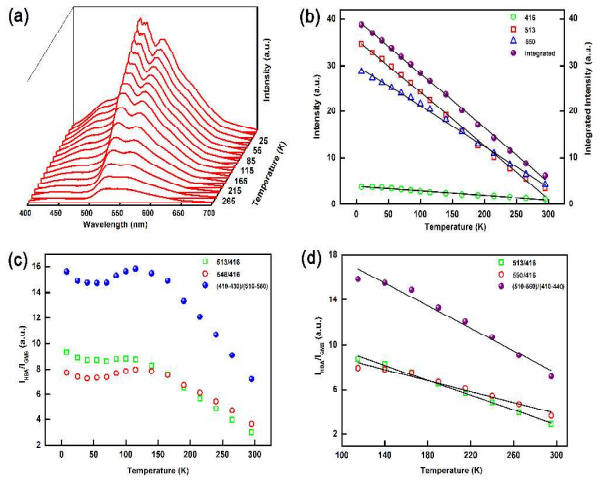

Figure3. (a) Fluorescence emission spectra of HBA-GMS at different temperature from 8 to 298 K. (b) Temperature dependence of fluorescence intensity (I_{416}, I_{513}, I_{550}) of HBA-GMS, showing the linear decrease in fluorescence intensity as a function of temperature at 8-298 K. Integrated fluorescence intensity as a function of temperature at 8-298 K for the HBA-GMS. (c) Fluorescence intensity ratio I_{HBA}/I_{GMS} (I_{513}/I_{416}, I_{550}/I_{416} and $I_{410-440}/I_{510-560}$) of HBA-GMS as a function of temperature. (d) Fluorescence intensity ratios I_{HBA}/I_{GMS} of HBA-GMS as a function of temperature at 100-298 K.

temperature from 8 to 298 K, which could be used for accurate temperature sensing (Figure3b). For HBA-GMS, as can be seen, the fluorescence intensity and the integrated fluorescence intensity change linearly with temperature in the range between 8 and 298 K representing. The results show that there is a good linear relation-ship between the PL intensity and temperature. To avoid the disturbance of HBA optical signals from the surroundings, we have plotted the ratio of the HBA emission to the gold nanoparticles emission as calibrated fluorescence part as a function of temperature. Figures 3d show the fluorescence intensity ratio (I_{513}/I_{416}, I_{550}/I_{416}) and the integrated intensity ($I_{510\text{-}560}/I_{410\text{-}440}$) as a function of temperature. As can be seen, a good linear correlation between the fluorescence intensity and integrated intensity ratio vs temperature from 100 to 298 K is observed as shown in Figure 3d. The ratio of I_{HBA}/I_{GMS} (I_{513}/I_{416}, I_{550}/I_{416} and $I_{510\text{-}560}/I_{410\text{-}440}$) on temperature from 100 to 298 K reveals a good linear relationship with a correlation coefficient of 0.97-0.99. The absolute temperature therefore can be linearly correlated to an experimental parameter Δ by Equation 1

$$\Delta = 22.467\text{-}0.0499T \quad (2)$$

Where $\Delta = I_{510\text{-}560}/I_{410\text{-}440}$ is the emission intensity ratio at different temperature between 100 and 300 K. This suggests that HBA-GMS are an excellent luminescent thermometer in this temperature range. As shown in Figure3d, the sensitivity of HBA-GMS is significantly enhanced and is higher than that of recently reported metal-organic framework.[11, 13] Such significantly enhanced sensitivity is really remarkable, which will allow us to highly sensitize the temperature changes.

The material biocompatibility is a key factor for their biological application. Thus, to fully evaluate possible toxicity of HBA and HBA-GMS, the cell viability of MEF (mouse embryo fibroblast) treated with different concentration of HBA and HBA-GMS for 24 hours was evaluated, respectively. The cells viability of MEF reduces from 82% to 38% when the concentration of HBA increases from 25 to 400 μg ml^{-1} as shown in Figure4. The cells viability of MEF maintains at around 100% when the concentration of HBA-GMS from 25 to 400 μg ml^{-1} (Figure4). It is concluded that HBA-GMS at the concentration up to 100 μg ml^{-1} does not shown significant toxicity in current experimental conditions. This may be attributed to that GMS is able to insulate and stabilize HBA molecules and therefore, inhibiting the possible interactions between HBA molecules and the surface of cells.

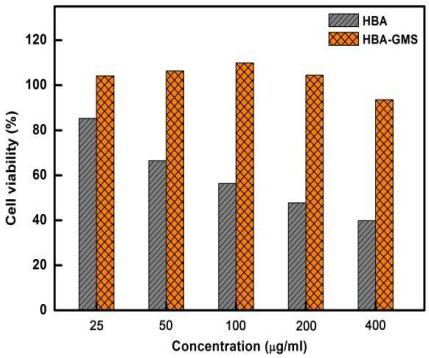

Figure4. Cell viability of B16 Cells in the presence of HBA (orange filled) and HBA-GMS (gray filled) evaluated using the MTT assay.

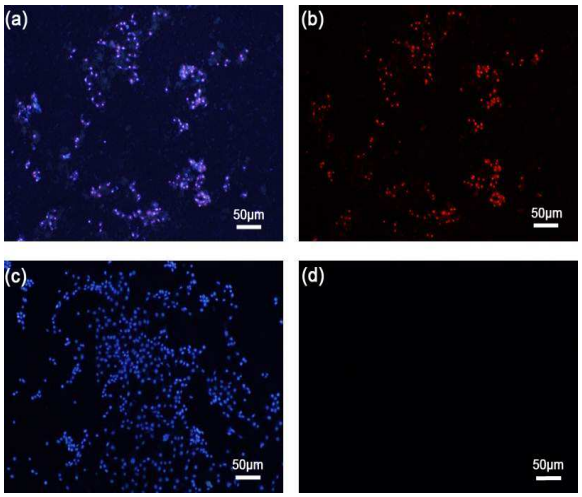

Figure5. Fluorescence images of B16 cells treated with HBA (a, b) and HBA-GMS (c, d). Hoechst 33342 are used to visualize the nuclei (blue a, c) and PI to illustrate the apoptotic cells (red b, d). (The amount of dead cells is expressed as the percentage of PI-positive cells).

To investigate the toxicity of HBA-GMS in skin cancer cell, a mixture of B16 cells (1.0×10^4 cells per well) are treated with HBA-GMS (100 μg ml^{-1}) for 5 hours (Figure5). Meanwhile, B16 cells are also incubated with HBA for 5 hours as a control samples (Figure5a and Figure5b). B16 cells grown in a medium are added with both PI (10 μg ml^{-1}) for staining the nuclei of dead cells) and Hoechst 33342 (5 μg ml^{-1}) for staining the nuclei of living cells, which are analyzed by using Image Pro for each condition. Cells that are treated with HBA show more cell death (Figure5a and 5b), whereas cells incubated with HBA-GMS are unaffected (Figure5c and Figure5d). Although the initial cell numbers are on the same level in all experiments, the staining procedure by trypan blue includes several washing steps. Thus, most of the cells incubated with HBA are discarded and result in the cell number difference comparing with that in HBA-GMS. Meanwhile, this wash process of the staining also prevents the influence of the sample fluorescence signal. In conclusion, HAB-GMS exhibit almost absent inhibitory effect on the viability and growth of cell suspension cultures in comparison with HBA without GMS. Since the HBA-GMS binds readily to the surface of cell, the reduction of HBA toxicity is owing to the protection of the mesoporous silica walls to avoid direct contact with cells. The result demonstrates that HBA-GMS exhibits low toxicity and provides a fluorescent thermometer tool for nanobio- technology, biomedicine, and animal fields.

Conclusions

In summary, a new temperature responsive salicylideneanilines (HBA), which is encapsulated within mesoporous silica functionalized gold nanoparticles (GMS) is demonstrated. HBA-

GMS as a calibrated fluorescent sensor shows strong and liner temperature-induced fluorescence intensity in the temperature range of 100 to 298 K. Moreover, GMS not only improves chemical stability and biocompatibility, but also eliminate the intrinsic toxicity of HBA effectively. GMS also improves the light harvesting and calibrates HBA fluorescence intensity in a wide temperature range because of the stable fluorescent signal of gold nanoparticle. Thus, HBA-GMS as temperature fluorescent thermometer can be used for colorimetric imaging. These properties make HBA-GMS a sensitive fluorescent colorimetric thermometer which can be used in many areas such as temperature distribution mapping.

Experimental

Preparation of HBA-GMS composites

4-(2-hydroxybenzylideneamino) benzoic acid (HBA) and GMS were synthesized by a previously reported procedure (see Supporting Information S1 for detailed experimental procedures).[35, 36] For a typical preparation, 2.5 mg of HBA was dissolved in 50 ml of ethanol first, followed by mixing 0.5 g of GMS in the solution for 12 hours at room temperature. The suspension was centrifuged and the transparent aqueous solution was decanted. The solid was carefully washed with ethanol to remove HBA and dried in a vacuum oven at 333 K. The solid powder was obtained and denoted as HBA-GMS.

In vitro cytotoxicity assay (MTT Assay)

The viability and proliferation of cells in the presence of HBA and HBA-GMS were evaluated by MTT assay by a previously reported procedure (see Supporting Information S1 for detailed experimental procedures).[41] Hoechst 33342/PI stain for cell death assay, hoechst 33342 is employed for staining of the cell nuclear and the red signal of PI indicated the dead cells. Cells treated with tested materials were stained with PI (0.5mg ml^{-1}) and Hoechst 33342 (5 μg ml^{-1}) for 20 min and washed with PBS for three times. All measurements in the experiments are made at room temperature.

Characterizations

Nuclear magnetic resonance (NMR) spectra were determined by using a Bruker AV300 NMR spectrometer (resonance frequency of 300 MHz for 1H) operated in the Fourier transform mode. CDCl3 was used as the solvent. The XRD patterns were recorded on a Philips X' Pert Pro Super diffractometer with Cu Kα radiation (λ = 1.54178 Å). The field emission scanning electron microscopy (FESEM) images were performed by using a FEI Sirion-200 scanning electron microscope. The transmission electron microscopy (TEM) images were taken on a JEOL-2010 TEM with an acceleration voltage of 200 kV. The porous textures of the samples were analyzed using nitrogen adsorption/desorption isotherms at 77 K. The nitrogen adsorption/desorption isotherms were determined by aapbp Micromeritics ASAP 2000 system. The FTIR spectra were measured on a NICOLET FT-IR spectrometer, using pressed KBr tablets. Thermal gravimetric analysis (TGA) of the samples were recorded on a Shimadzu TA-50 thermal analyzer at a heating rate of 10 °C/min from room temperature to 800 °C in air. UV-Vis spectra were carried out on a Solid Spec-3700 spectrophotometer at room temperature. Fluorescence measurements were determined by the FluoRoLOG-3-TAU (Jobin Yvon, France) fluorescence spectrometer, which was produced by a xenon lamp equipped with a grating monochromator. Low temperatures were achieved by CCS-355 (Janis, American) low temperature equipment.

Acknowledgements

This work is financially supported from the Agency for Science, Technology and Research (A*STAR) and Ministry of National Development (MND) Singapore (grant #: SERC 1321760014). We would like to acknowledge the partial support by the National Natural Science Foundation of China (No. 51302282).

Notes and references

1 C. D. S. Brites, P. P. Lima, N. J. O. Silva, A. Millan, V. S. Amaral, F. Palacio and L. D. Carlos, *Nanoscale*, 2012, **4**, 4799-4829.
2 X. D. Wang, O. S. Wolfbeis and R. J. Meier, *Chem Soc Rev*, 2013, **42**, 7834-7869.
3 G. Kucsko, P. C. Maurer, N. Y. Yao, M. Kubo, H. J. Noh, P. K. Lo, H. Park and M. D. Lukin, *Nature*, 2013, **500**, 54-U71.
4 D. Cauzzi, R. Pattacini, M. Delferro, F. Dini, C. Di Natale, R. Paolesse, S. Bonacchi, M. Montalti, N. Zaccheroni, M. Calvaresi, F. Zerbetto and L. Prodi, *Angew Chem Int Edit*, 2012, **51**, 9662-9665.
5 D. Zhou, M. Lin, X. Liu, J. Li, Z. L. Chen, D. Yao, H. Z. Sun, H. Zhang and B. Yang, *Acs Nano*, 2013, **7**, 2273-2283.
6 Y. Takei, S. Arai, A. Murata, M. Takabayashi, K. Oyama, S. Ishiwata, S. Takeoka and M. Suzuki, *Acs Nano*, 2014, **8**, 198-206.
7 C. H. Hsia, A. Wuttig and H. Yang, *Acs Nano*, 2011, **5**, 9511-9522.
8 E. J. McLaurin, V. A. Vlaskin and D. R. Gamelin, *J Am Chem Soc*, 2011, **133**, 14978-14980.
9 V. A. Vlaskin, N. Janssen, J. van Rijssel, R. Beaulac and D. R. Gamelin, *Nano Lett*, 2010, **10**, 3670-3674.
10 J. Feng, K. J. Tian, D. H. Hu, S. Q. Wang, S. Y. Li, Y. Zeng, Y. Li and G. Q. Yang, *Angew Chem Int Edit*, 2011, **50**, 8072-8076.
11 X. T. Rao, T. Song, J. K. Gao, Y. J. Cui, Y. Yang, C. D. Wu, B. L. Chen and G. D. Qian, *J Am Chem Soc*, 2013, **135**, 15559-15564.
12 S. S. Babu, M. J. Hollamby, J. Aimi, H. Ozawa, A. Saeki, S. Seki, K. Kobayashi, K. Hagiwara, M. Yoshizawa, H. Mohwald and T. Nakanishi, *Nat Commun*, 2013, **4**.
13 Y. J. Cui, H. Xu, Y. F. Yue, Z. Y. Guo, J. C. Yu, Z. X. Chen, J. K. Gao, Y. Yang, G. D. Qian and B. L. Chen, *J Am Chem Soc*, 2012, **134**, 3979-3982.
14 C. Gota, K. Okabe, T. Funatsu, Y. Harada and S. Uchiyama, *J Am Chem Soc*, 2009, **131**, 2766-2767.
15 E. Hadjoudis and I. M. Mavridis, *Chem Soc Rev*, 2004, **33**, 579-588.
16 P. L. Jacquemin, K. Robeyns, M. Devillers and Y. Garcia, *Chem Commun*, 2014, **50**, 649-651.

17 K. M. Hutchins, S. Dutta, B. P. Loren and L. R. MacGillivray, *Chem Mater*, 2014, **26**, 3042-3044.
18 F. Robert, A. D. Naik, B. Tinant, R. Robiette and Y. Garcia, *Chem-Eur J*, 2009, **15**, 4327-4342.
19 F. Robert, P. L. Jacquemin, B. Tinant and Y. Garcia, *Crystengcomm*, 2012, **14**, 4396-4406.
20 T. Haneda, M. Kawano, T. Kojima and M. Fujita, *Angew Chem Int Edit*, 2007, **46**, 6643-6645.
21 J. Harada, T. Fujiwara and K. Ogawa, *J Am Chem Soc*, 2007, **129**, 16216-16221.
22 M. Sliwa, N. Mouton, C. Ruckebusch, L. Poisson, A. Idrissi, S. Aloise, L. Potier, J. Dubois, O. Poizata and G. Buntinx, *Photoch Photobio Sci*, 2010, **9**, 661-669.
23 R. Alford, H. M. Simpson, J. Duberman, G. C. Hill, M. Ogawa, C. Regino, H. Kobayashi and P. L. Choyke, *Mol Imaging*, 2009, **8**, 341-354.
24 B. B. Brodie, W. D. Reid, A. K. Cho, G. Sipes, G. Krishna and J. R. Gillette, *P Natl Acad Sci USA*, 1971, **68**, 160-164.
25 J. L. Gao, *Accounts Chem Res*, 1996, **29**, 298-305.
26 S. Draxler and M. E. Lippitsch, *Anal Chem*, 1996, **68**, 753-757.
27 J. Feng, L. Xiong, S. Q. Wang, S. Y. Li, Y. Li and G. Q. Yang, *Adv Funct Mater*, 2013, **23**, 340-345.
28 L. A. Muhlstein, J. Sauer and T. Bein, *Adv Funct Mater*, 2009, **19**, 2027-2037.
29 H. S. Peng, M. I. J. Stich, J. B. Yu, L. N. Sun, L. H. Fischer and O. S. Wolfbeis, *Adv Mater*, 2010, **22**, 716-719.
30 Q. N. Lin, Q. Huang, C. Y. Li, C. Y. Bao, Z. Z. Liu, F. Y. Li and L. Y. Zhu, *J Am Chem Soc*, 2010, **132**, 10645-10647.
31 S. Inagaki, O. Ohtani, Y. Goto, K. Okamoto, M. Ikai, K. Yamanaka, T. Tani and T. Okada, *Angew Chem Int Edit*, 2009, **48**, 4042-4046.
32 L. F. Chen, J. C. Hu, Z. W. Qi, Y. J. Fang and R. Richards, *Ind Eng Chem Res*, 2011, **50**, 13642-13649.
33 L. F. Chen, J. C. Hu and R. Richards, *J Am Chem Soc*, 2009, **131**, 914-915.
34 E. J. McLaurin, L. R. Bradshaw and D. R. Gamelin, *Chem Mater*, 2013, **25**, 1283-1292.
35 F. D. Jochum and P. Theato, *Macromolecules*, 2009, **42**, 5941-5945.
36 K. Johmoto, A. Sekine and H. Uekusa, *Cryst Growth Des*, 2012, **12**, 4779-4786.
37 J. Wu, L. W. Liao, W. S. Yan, Y. Xue, Y. F. Sun, X. Yan, Y. X. Chen and Y. Xie, *Chemsuschem*, 2012, **5**, 1207-1212.
38 V. C. M. Avadanei, S. Shova, J. A. Paixão, *Chem Phys*, 2014, **444**, 43-51.
39 L. Chen, J. Hu, R. Richards. *J. Am. Chem. Soc*. 2009, **131**, 914-915.
40 J. Wu, L. Liao, W. Yan, Y. Xue, Y. Sun, X. Yan, Y. Chen and Y. Xie, *ChemSusChem,* 2012, **5**, 1207-1212.
41 J. Wu, W. Zhou, Q. Cheng, J. Yang, *RSC Adv*. 2015, **5**, 22965-22971.